Tectonophysics 728–729 (2018) 75–91

Contents lists available at ScienceDirect

Tectonophysics

journal homepage: www.elsevier.com/locate/tecto

Off-axis volcano-tectonic activity during continental rifting: Insights from the transversal Goba-Bonga lineament, Main Ethiopian Rift (East Africa)

Giacomo Corti[a,b,*], Federico Sani[c], Samuele Agostini[d], Melody Philippon[e,f], Dimitrios Sokoutis[e,g], Ernst Willingshofer[e]

[a] Consiglio Nazionale delle Ricerche, Istituto di Geoscienze e Georisorse, UOS Firenze, via G. La Pira 4, 50121 Firenze, Italy
[b] Istituto Nazionale di Geofisica e Vulcanologia, Sezione di Pisa, Via della Faggiola, 32, 50126 Pisa, Italy
[c] Dipartimento di Scienze della Terra, Università degli Studi di Firenze, via G. La Pira 4, 56124 Firenze, Italy
[d] Consiglio Nazionale delle Ricerche, Istituto di Geoscienze e Georisorse, Via G. Moruzzi 1, 56124 Pisa, Italy
[e] Utrecht University, Faculty of Earth Sciences, Department of Tectonics, Budapestlaan 6, 3584 CD Utrecht, The Netherlands
[f] Gesociences Montpellier, UMR CNRS 5243, Université des Antilles, 97170 Pointe-à-Pitre, French West Indies, France
[g] University of Oslo, Department of Geosciences, PO Box 1047 Blindern, N-0316 Oslo, Norway

ARTICLE INFO

Keywords:
Continental rifting
Main Ethiopian Rift
Transversal lineaments
Off-axis
Pre-existing structures

ABSTRACT

The Main Ethiopian Rift, East Africa, is characterized by the presence of major, enigmatic structures which strike approximately orthogonal to the trend of the rift valley. These structures are marked by important deformation and magmatic activity in an off-axis position in the plateaus surrounding the rift. In this study, we present new structural data based on a remote and field analysis, complemented with analogue modelling experiments, and new geochemical analysis of volcanic rocks sampled in different portions of one of these transversal structures: the Goba-Bonga volcano-tectonic lineament (GBVL). This integrated analysis shows that the GBVL is associated with roughly E–W-trending prominent volcano-tectonic activity affecting the western plateau. Within the rift floor, the approximately E–W alignment of Awasa and Corbetti calderas likely represent expressions of the GBVL. Conversely, no tectonic or volcanic features of similar (E–W) orientation have been recognized on the eastern plateau. Analogue modelling suggests that the volcano-tectonic features of the GBVL have probably been controlled by the presence of a roughly E–W striking pre-existing discontinuity beneath the western plateau, which did not extend beneath the eastern plateau. Geochemical analysis supports this interpretation and indicates that, although magmas have the same sub-lithospheric mantle source, limited differences in magma evolution displayed by products found along the GBVL may be ascribed to the different tectonic framework to the west, to the east, and in the axial zone of the rift. These results support the importance of the heterogeneous nature of the lithosphere and the spatial variations of its structure in controlling the architecture of continental rifts and the distribution of the related volcano-tectonic activity.

1. Introduction

The relation between pre-existing structures affecting continental lithosphere and the architecture of rift systems is fundamental for understanding the dynamics of extension and rupture of the continental plates. The presence of inherited pervasive or discrete fabrics has been shown to exert a primary control on the extension-related pattern of deformation at both regional and local scale (e.g., Ziegler and Cloetingh, 2004; Bellahsen and Daniel, 2005; Sokoutis et al., 2007; Corti, 2012; Brune, 2016). In particular, transverse pre-existing anisotropies have been shown to have a significant influence on rift architecture, by controlling rift propagation, interaction and segmentation (Rosendahl, 1987; Morley et al., 1990; Faulds and Varga, 1998; Michon and Sokoutis, 2005; Laó-Dávila et al., 2015; Corti et al., 2018a), or the fault pattern at a more local scale (e.g., Le Turdu et al., 1999; Lezzar et al., 2002; Sokoutis et al., 2007; Corti et al., 2007). Pre-existing structures may also have a dominant role in the distribution of deformation both within and outside the rift valley (e.g., Abebe et al., 1998).

The Main Ethiopian Rift (MER), in East Africa, is a classical example where several pre-rift deformation events, from collision during the Precambrian to Mesozoic extension (e.g., Abbate et al., 2015), gave rise to differently-oriented fabrics which have controlled the subsequent Cenozoic extension. Among these fabrics, major E–W anisotropies,

* Corresponding author at: Istituto Nazionale di Geofisica e Vulcanologia, Sezione di Pisa, Via della Faggiola, 32, 50126 Pisa, Italy.
E-mail address: giacomo.corti@igg.cnr.it (G. Corti).

https://doi.org/10.1016/j.tecto.2018.02.011
Received 23 August 2017; Received in revised form 12 February 2018; Accepted 13 February 2018
Available online 16 February 2018

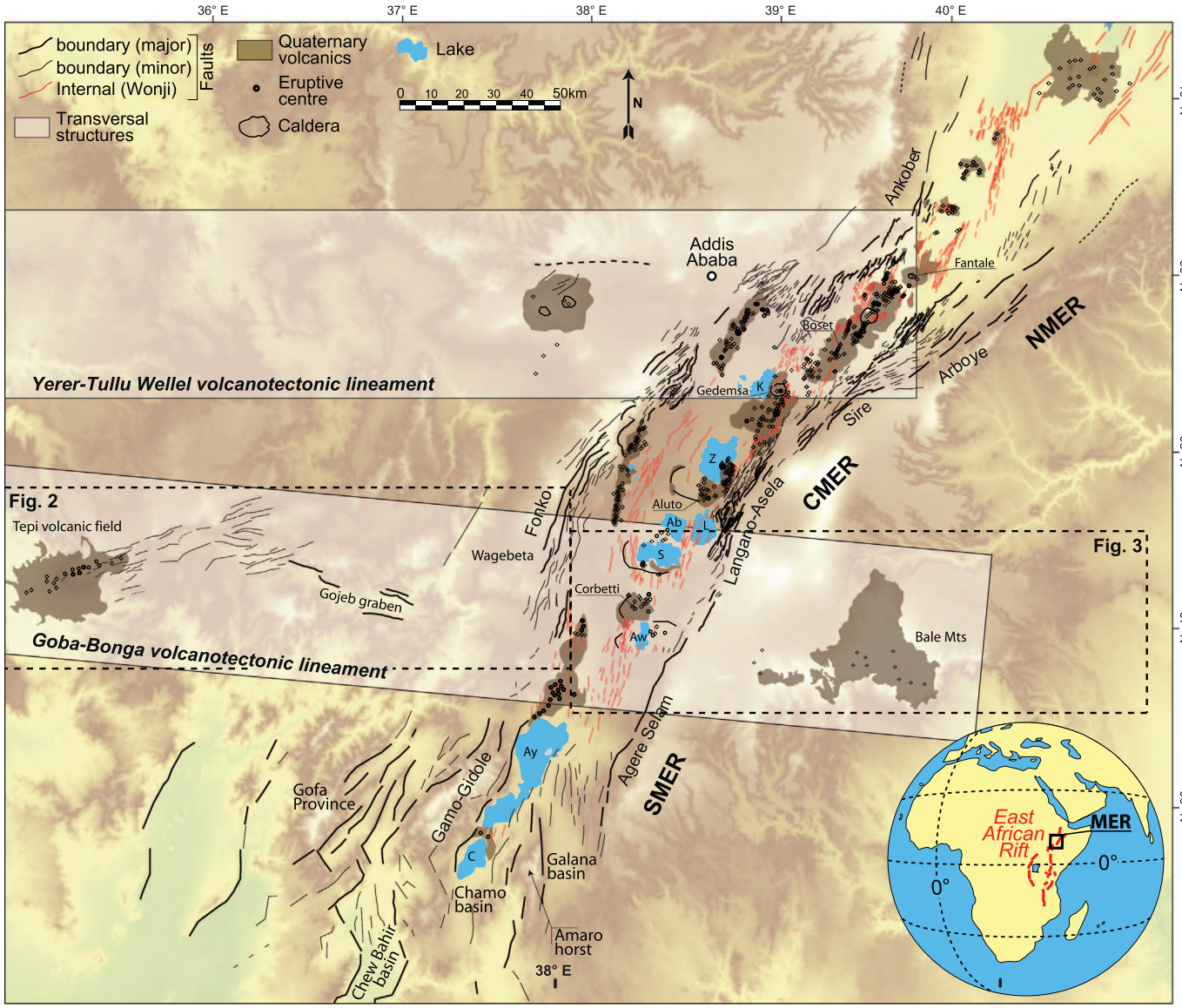

Fig. 1. Tectonic setting of the Main Ethiopian Rift (MER) superimposed on a NASA's Shuttle Radar Topography Mission (SRTM) digital elevation model. The white rectangles indicate the extent of the two major volcano-tectonic lineaments of Yerer-Tullu Wellel and Goba Bonga. Quaternary volcanics modified from Abebe et al. (1998), Berhe et al. (1987), Corti (2009), Davidson (1983), Moore and Davidson (1978), Tefera et al. (1996). CMER: Central Main Ethiopian Rift; NMER: Northern Main Ethiopian Rift; SMER: Southern Main Ethiopian Rift. Lakes are labeled as follows: Ab: Abyata; Ay: Abaya; Aw: Awasa; C, Chamo; K, Koka; L, Langano; Sh, Shala; Z, Ziway.

roughly orthogonal to the trend of the rift valley, have been suggested to exert a significant control on the distribution of the rift-related volcano-tectonic activity, causing important deformation and magmatic activity in a marked off-axis position in the plateaus surrounding the rift (e.g., Abbate and Sagri, 1980; Abebe et al., 1998; Abebe Adhana, 2014).

In this contribution, we improve the current knowledge of one of the most important -yet poorly known- transverse structures, the Goba-Bonga volcano-tectonic lineament (Abbate and Sagri, 1980), at the boundary between the Central and the Southern MER (Fig. 1). We do this by (1) providing new constraints on its volcano-tectonic architecture, lateral extent and kinematics, and (2) analysing the influence of pre-existing structures on its characteristics. To this end, we complement the few existing works by using a new dataset combining: (i) structural analysis based on both remote analysis and fieldwork, (ii) analogue modelling, and (iii) new geochemical analysis of volcanic rocks sampled in different portions of this transversal structure.

2. Tectonic setting

The MER represents the northern termination of the East African Rift System and extends from Afar in the north, to the Turkana depression in the south (Fig. 1). It is a region of rifting that accommodates the active extension between the major Nubia and Somalia Plates (e.g. Ebinger, 2005; Corti, 2009), which is occurring in a roughly E–W direction at rates of ~4–6 mm/yr (e.g., Saria et al., 2014). The MER is traditionally subdivided into three main sectors (Northern MER; Central MER and Southern MER; Fig. 1), whose variations in style of extension have been interpreted to reflect different stages in the evolutionary rift sequence, from fault-dominated initial rifting in the Southern MER to magma-dominated incipient break-up in the Northern MER (e.g., Hayward and Ebinger, 1996; Corti, 2009; Agostini et al., 2011; Keir et al., 2013).

The transition between these different rift segments is defined by the occurrence of major structures transverse to the rift trend that may extend for hundreds of kilometers away from the rift margins on both the Somalian and Ethiopian plateaus. A typical example is the well-

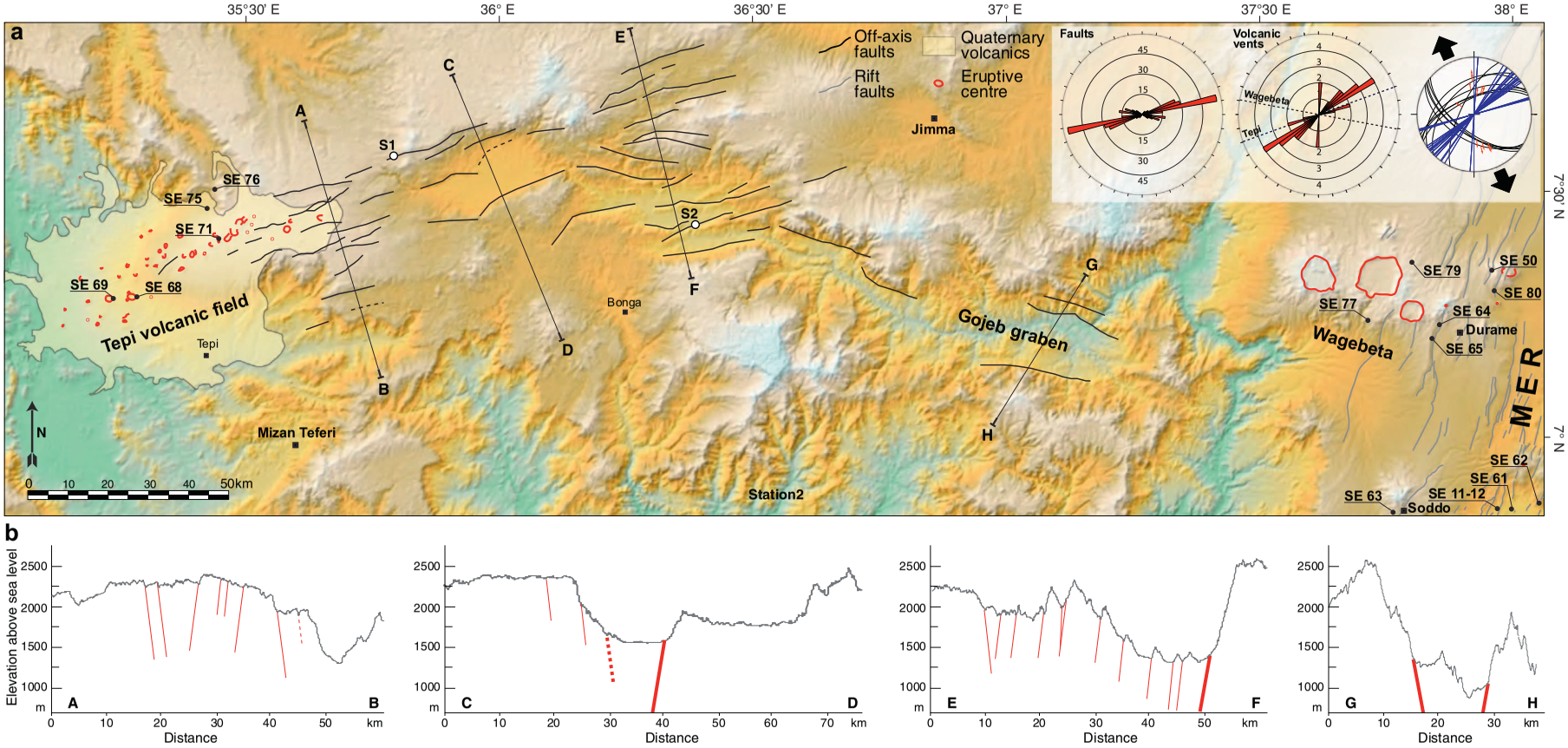

Fig. 2. (a) Digital elevation model of the Ethiopian plateau in the Wagebeta-Tepi area with superimposed faults affecting the plateau (black lines), faults of the rift valley (grey lines) and the contour of volcanic vents (red lines). The extent of the Quaternary volcanic field is reported (modified from Moore and Davidson, 1978; Davidson, 1983). Rose diagram illustrating plots of weighted fault azimuth and elongation of volcanic vents in the volcanic field are reported as insets; black dashed lines indicate the overall elongation of the field and that of the Wagebeta calderas. Labels on the axis of the rose diagram indicate the number of faults or volcanic vents falling within a given azimuth bin. Stereographic projection (Schmidt net, lower hemisphere) displays the fault planes (black lines) with the collected associated fault-slip vectors (red arrows) and the trend of alignments of volcanic vents (blue lines); black arrows indicate the obtained direction of extension by using the P& T axes inversion method (calculated with Win-Tensor, Delvaux and Sperner, 2003). White dots labeled "S + number" indicate the sites of structural measurements; black dots labeled "SE + number" indicate rock samples. MER: Main Ethiopian Rift. (b) Topographic profiles extracted from the digital elevation model with major and minor normal faults indicated by thick and thin red lines, respectively. (For interpretation of the references to color in this figure legend, the reader is referred to the web version of this article.)

known Yerer-Tullu Wellel Volcano-tectonic Lineament (YTVL; e.g., Abebe et al., 1998), which extends for about 700 km from the western rift margin to Tullu Wellel near the Ethiopia-Sudan border, and separates the Northern MER from the Central MER (Fig. 1). The YTVL consists of a tectono-magmatic system characterized by a roughly E–W alignment of normal faults and major volcanic centres (e.g., Abebe et al., 1998; Tommasini et al., 2005; Abebe Adhana, 2014), interpreted to result from Cenozoic reactivation pre-existing Neoproterozoic structures sub-parallel to the trend of the Gulf of Aden (e.g., Abebe et al., 1998; Korme et al., 2004; Abebe Adhana, 2014).

Another major E–W-trending transverse lineament is the Goba-Bonga volcano-tectonic lineament (GBVL; e.g., Merla et al., 1979; Abbate and Sagri, 1980), which separates the Central MER from the Southern MER (Fig. 1). Similarly to the YTVL, this structure is characterized by the occurrence of normal faults and associated volcanic centres of Pliocene-recent age. At the westernmost termination of the structure, the Tepi volcanic field is made of large sub-horizontal, shield-forming columnar basaltic flows, which in places have flowed down pre-existing valleys; prominent cinder cones and collapse craters lie along the ENE–WSW-trending central axis of the shield (Fig. 2; e.g., Moore and Davidson, 1978; Davidson, 1983; Ayalew et al., 2006). Although the age of the volcanic field is not known, its relatively fresh geomorphological expression in a region of high rainfall and the presence of active hot springs associated with this volcanism suggest a recent age, most likely Holocene (e.g., Moore and Davidson, 1978; Davidson, 1983). Moore and Davidson (1978) suggest the Tepi volcanic field to have been built from fissural eruptions along ENE–WSW-trending faults. East of Tepi, the GBVL is well expressed in the western plateau by an array of ENE–WSW faults in the Jimma area (Moore and Davidson, 1978; Davidson, 1983; Berhe et al., 1987) and by the Gojeb graben, a ESE–WNW fault-bounded depression (Fig. 2; e.g., Bonini et al., 2005). Further to the east, the Wagebeta volcanic complex is formed by a roughly E–W alignment of Pliocene large calderas and associated domes (Fig. 2); the transverse arrangement to the rift margin has been referred to the control exerted by structures belonging to the GBVL (e.g., Merla et al., 1979; WoldeGabriel et al., 1990). Similarly, within the rift valley, the typical elongation of some Pliocene-recent calderas (Awasa, Corbetti; Fig. 3) has been related to the existence of pre-existing E–W discontinuities (e.g., Acocella et al., 2002). On the eastern plateau, volcanism is more diffuse and dominated by the occurrence of large off-axis volcanic centres, such as the Galama range, Kaka and Hunkuolo, which are Middle-Late Pliocene in age and mainly of basaltic and trachytic composition (Fig. 3; Mohr and Potter, 1976; WoldeGabriel et al., 1990). Mohr and Potter (1976) indicated alignment of these volcanic centres in a NNE-SSW direction, likely reflecting the structural control exerted by pre-existing crustal weaknesses. Several Plio-Quaternary scoria cones are widespread in the Somalian plateau in the surroundings of these major volcanic centres. The volcanic complex of the Bale Mountains is believed to characterize the eastern termination of the GBVL (Fig. 3; Abbate and Sagri, 1980). This large, composite volcanic complex is made of basaltic units overlain by trachytes. It has been built in two distinct volcanic episodes: an early episode, likely related to the emplacement of the trap series, during the Oligocene (at ~26–25 Ma), and a later episode during the Pleistocene (~1.6–0.7 Ma; e.g., Nelson, 2009).

As suggested for the YTVL, the GBVL has been likely controlled by pre-existing weaknesses transversal to the rift valley (e.g., Abbate and Sagri, 1980; Abebe Adhana, 2014; see also below Section 5).

3. Volcano-tectonic features of the Goba-Bonga volcano-tectonic lineament

3.1. Methods

The characteristics of the volcano-tectonic activity associated with the BGVL were analysed through integration of remote sensing and field work. Remote analysis was based on interpretation of satellite imagery (Landsat TM, Aster and other available images, e.g., Google Earth imagery) and digital elevation models (DEMs; Nasa's Shuttle Radar Topography Mission, SRTM, 30 m–resolution). The aims of this remote sensing study were: 1) detailed mapping of fault traces, 2) morpho-tectonic analysis of the main structures (e.g., definition of the morphological offset of faults), 3) first-order definition of the relations between structures and volcanic centres, and 4) selection of key-areas for the fieldwork. This latter activity was conducted during different field surveys between 2010 and 2013, and consisted of: 1) analysis of the morpho-tectonic structures recognized through the remote sensing study, 2) structural analysis of the fault planes, 3) a more detailed investigation of the relations between faulting and volcanism and 4) sampling of volcanic rocks for geochemical analysis (see below Section 5).

In order to better characterize the distribution of volcanic vents in the area, vent alignments were mapped according to the procedure illustrated in Paulsen and Wilson (2010). Vent mapping has been performed on available satellite images (mostly Google Earth imagery) and DEMs. Specifically, vent alignments have been mapped based on of the spatial distribution of vents as well as their shapes (vent elongation provides a critical parameter to group single vents into an alignment).

Kinematic indicators on fault planes (i.e., fault slip data such as striae) and strikes and dip of faults were measured in two different sites on the Tepi fault system (Fig. 2a). These fault slip data and/or the orientation of vent alignments (assuming that these alignments are representative of feeding dykes; e.g., Paulsen and Wilson, 2010) data were elaborated in order to calculate paleostress axes orientations through the P&T axes inversion method (calculated with Win-Tensor, Delvaux and Sperner, 2003).

3.2. Western plateau

The area affected by the GBVL on the western plateau extends from the margin of the rift valley north of Soddo to Mizan Teferi in the west (Fig. 2). Our new structural analysis (Fig. 2) indicates diffuse deformation in the area between Jimma and Mizan Teferi, with several normal faults affecting an area > 40 km-wide in places (Fig. 2). The faults have generally morphological offset of < 500 m, although some faults may reach offsets of ~1000 m (Fig. 2b). These faults define a few minor topographic depressions oriented roughly ENE–WSW. There are no indications for the timing of activity of these faults; however, our fieldwork and analysis of satellite images and DEMs indicate prominent morphological expression with presence of typical morphotectonic features (e.g., continuous, preserved scarps), suggesting a recent activity. This recent activity is also supported by displacement of Quaternary lavas of the Tepi volcanic field, north and northeast of Tepi (Fig. 2a). However, the limited number of faults affecting the volcanic products likely indicates that most of the deformation occurred prior to Quaternary times.

To the west, the Gojeb graben is instead characterized by more localised deformation; normal faults define indeed a narrow (20–25 km-wide) depression bordered by a few, WNW-ESE-striking normal faults, with large vertical offset (> 500 m; Fig. 2b). The architecture of the Gojeb graben is characterized by a roughly symmetric basin in the east transitioning to an asymmetric graben, with a master fault on the northern side, in the west (Fig. 2). Prominent morphological expression of some fault segments and the presence of typical morphotectonic features (e.g., continuous fresh scarps, triangular facets), suggest a recent activity of at least parts of these fault systems.

Analysis of weighted fault orientation indicates the existence of two main fault populations, as indicated by the two peaks in the rose diagram of fault distribution in Fig. 2a. The main peak, with orientation ~N75–80°E, corresponds to the faults of the Jimma-Mizan Teferi domain, whereas the minor peak at ~N95–100°E reflects boundary faulting of the Gojeb graben (Fig. 2a; Table 1). Statistical analysis of the

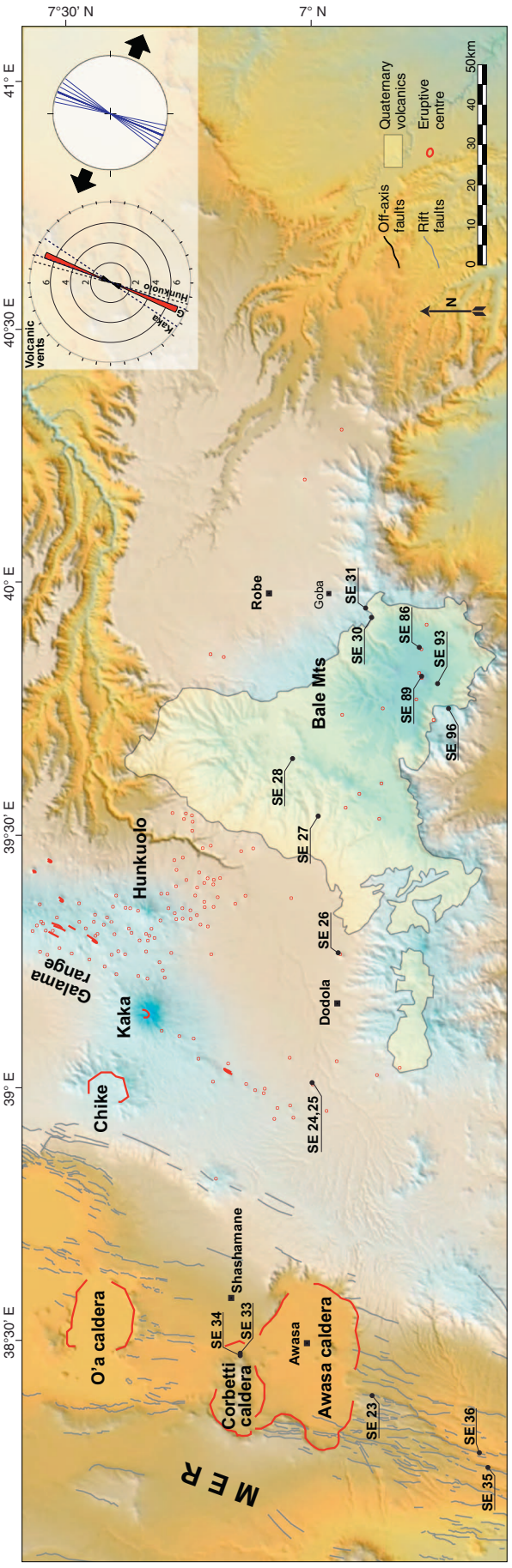

Fig. 3. Digital elevation model of the Somalian plateau in the Bale Mountains region and volcano-tectonic features illustrated as in Fig. 2. The extent of the Quaternary volcanism in the Bale Mountains volcanic field is reported (modified from Berhe et al., 1987; Tefera et al., 1996). Rose diagram illustrating plots of elongation of volcanic vents in the region are reported as insets; black dashed lines indicate the overall elongation of the Kaka, Hunkuolo and Galama Range (G) fields. Stereographic projection illustrates the obtained direction of extension from inversion of the trend of alignments of volcanic vents as in Fig. 2.

Table 1
Fault distribution, kinematics and alignment of volcanic vents/fields in the western and eastern plateaus.

	Weighted fault azimuths	Alignment of volcanic vents	Elongation of the volcanic field	Extension direction from inversion of fault data and/or volcanic alignments
Western plateau	Main peak: N75–80°E (minor peak: N95–100°E)	Main peak: N55–60°E (minor peaks: N0–5°E and N70–75°E)	Tepi: ~N70°E Wagebeta: ~N100°E	~N155°E
Eastern plateau	–	Main peak: N20–25°E	Galama: ~N20°E Hunkuolo: ~N15°E Kaka: ~N35°E	~N114°E

distribution of volcanic vents indicates that the majority of these vents are aligned in an ENE–WSW direction (main peak in the rose diagram in Fig. 2a oriented at N55–60°E; Table 1), which roughly corresponds to the overall elongation of the Tepi Quaternary basaltic shield. Minor peaks in the diagram of vent distribution occur at N0–5°E and N70–75°E (Fig. 2a, Table 1). The peaks at N55–60°E and N70–75°E overlap with the orientations of the faults affecting the area, supporting a close relationship between the faults affecting this portion of the western plateau and the recent volcanism. Conversely, the N—S peak does not overlap with fault orientations indicating that other processes (e.g., influence of pre-existing discrete basement weaknesses, perturbation of the regional stress field induced by load of volcanic edifices and/or overpressured magma reservoirs; e.g., Wadge et al., 2016) may have contributed to locally control vent orientation. It is worth to note that the Wagebeta caldera complex, located on the western rift margin, shows an WNW-ESE alignment that is exactly in line with the main faults bounding the Gojeb graben, about 50 km to the west (Merla et al., 1979).

Elaboration of fault-slip data and the alignment of volcanic vents indicate extension in a roughly NNW-SSE direction (Fig. 2a; Table 1).

3.3. Eastern plateau

Structural analysis on the eastern plateau indicates that, in contrast to the western plateau, this area is characterized by lack of any significant faulting (Fig. 3). The only faults affecting the Somalian highlands are a few NNE-SSW faults related to deformation of the rift margin SW of Chike. Instead, widespread Pliocene-recent volcanism in the Kaka-Hunkuolo-Galama Range centres and at the Bale Mountains affected the area. Although there exists an apparent E–W alignment between Chike, Kaka and Hunkuolo, the disparity in age of these centres (~11–12 Ma for Mt. Chike and ~2–3 Ma for Mts. Kaka and Hunkuolo; WoldeGabriel et al., 1990) suggests that the development of Chike is unrelated to the others. Our new statistical analysis clearly highlights indeed a preferential NNE-SSW (N20–25°E) alignment, which matches the overall orientation of the Kaka, Hunkuolo and Galama range fields (Fig. 3; Table 1). Differently from these centres, alignments or significant elongation of volcanic vents have not been recognized in the Bale Mountains.

In general, no influence of pre-existing E–W fabrics has been observed in the eastern plateau.

Elaboration of the alignment of volcanic vents indicate extension in a roughly ESE–WNW direction (Fig. 3; Table 1).

3.4. Along-axis differences in rift structure and margin characteristics

Analysis of the rift structure in the Central/Southern MER (Fig. 4) reveals the existence of an anomalous architecture of the western margin between Soddo and the Wagebeta complex, in the area corresponding to the GBVL. This region is characterized by the lack of a major rift escarpment and a smooth transition between the rift floor and the western plateau (whose difference in elevation is ~500 m) accommodated by numerous faults with limited vertical offset (Corti et al., 2013a). This marks a significant difference in margin architecture with respect to the adjacent Fonko-Guraghe and Chencha-Arba Minch areas, where a few boundary faults with large vertical offset (up to >1000 m) give rise to prominent fault escarpments (up to ~1500 m in height; Fig. 4b). These variations indicate a prominent along-axis variation in rift structure. At the latitude of the GBVL, rifting is asymmetric, with a major boundary fault system on the eastern margin with no counterpart on the opposite side (section CD in Fig. 4b). This is in contrast with the more symmetric nature of the rift to the north and south, as exemplified by the transect crossing the rift at the latitude of the Fonko-Guraghe and Langano-Asela escarpments (section AB in Fig. 4b).

South of the GBVL, the western plateau is affected by widespread deformation in the so-called Gofa Basin and Range and extension-related deformation is diffused over an area larger than 200 km wide, characterized by a complex topography (e.g., Moore and Davidson, 1978). North of this structure the plateau is instead more or less undeformed and extension is only accommodated within the rift valley (i.e., in an area which is <100 km wide). No significant deformation affects the eastern plateau either south or north of the supposed GBVL.

These along-axis variations in margin architecture are also reflected in the topography of the rift margins. To describe and quantify the general topographic trend of the margins we generated two rift-parallel swath profiles (Fig. 4c), which show the trend of maximum, minimum and mean elevation in a single plot (Isacks, 1992). We extracted them from the SRTM digital elevation models in GIS environment, sampling topography every 2 km into observation windows 25 km wide. This analysis shows important variations in elevation of the western plateau (Fig. 4c). The area corresponding to the GBVL shows a mean elevation of 1400–2000 m as in the Soddo-Durame area, increasing to 2000–2500 m asl in the surrounding areas (e.g., Fonko-Guraghe and Chencha; Fig. 4c). Conversely, the topography and architecture of the eastern rift margin are more regular, with a large bounding escarpment characterizing the Central/Southern MER and no significant changes in the area corresponding to the supposed GBVL (Fig. 4).

4. Analogue modelling

4.1. Rationale and set-up

The above observations argue against the existence of a continuous structure extending from the area on the western plateau to the Bale area on the eastern plateau; i.e., our data do not support the existence of continuous GBVL transecting the rift and affecting both plateaus. Conversely, these data suggest that a roughly E–W structure affects the western plateau between Tepi volcanic field and the western margin, likely continuing eastwards into the rift valley up to the roughly E–W-trending Awasa caldera but not affecting the eastern margin. We performed a series of analogue models to assess this interpretation and to analyse the possible influence on rifting of the presence of an inherited discontinuity, orthogonal to the rift valley, beneath the western plateau

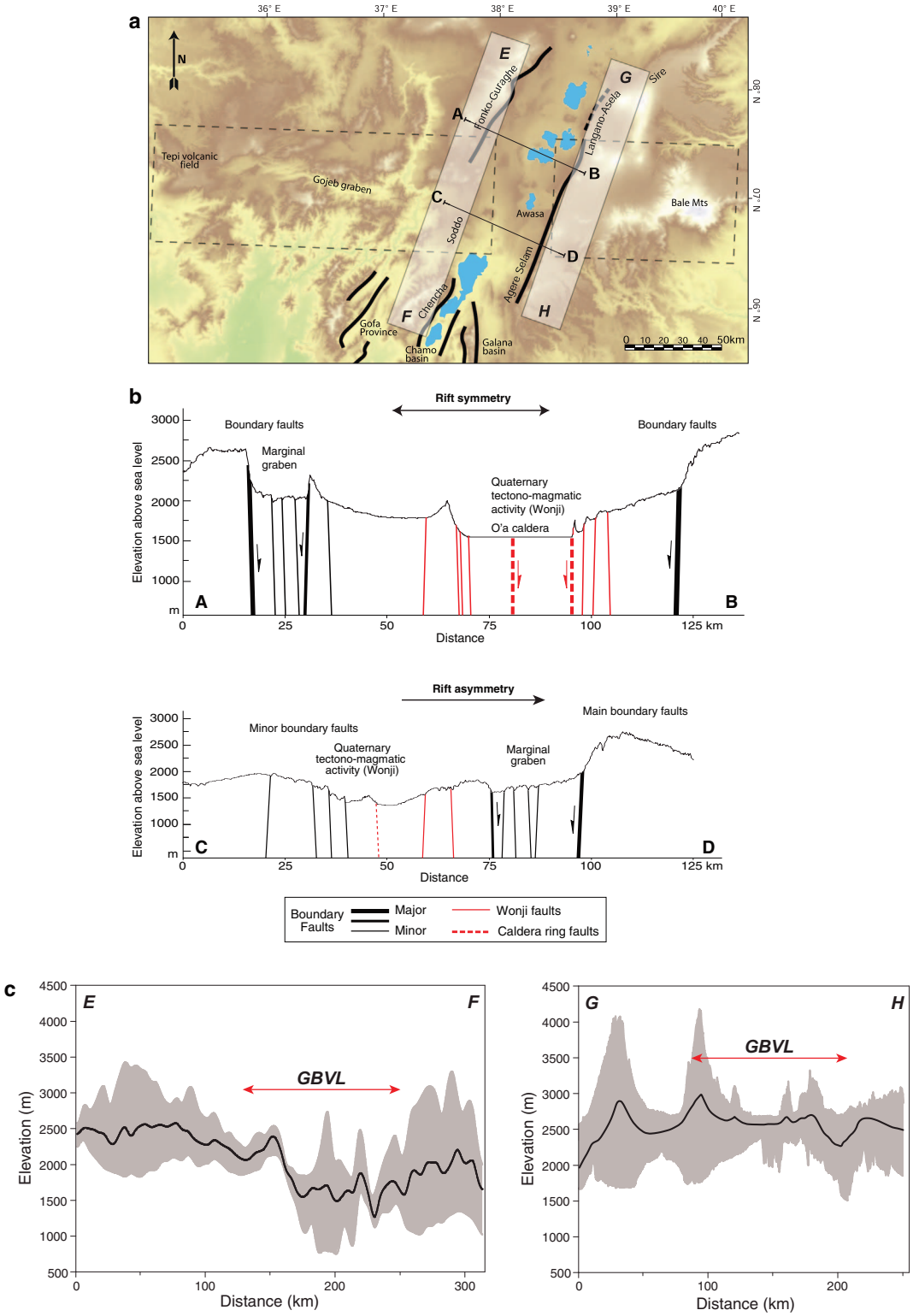

Fig. 4. Location map (a) of structural cross-sections (A–B, C–D) of the rift valley (b) and swath profiles (E–F, G–H) illustrating the average topography of the rift margins (c). In panel (b) note the transition from a symmetric structure at the latitude of the Guraghe and Asela-Langano escarpments (section A–B) to an asymmetric structure at the latitude of the GBVL (section C–D) (modified from Corti et al., 2018a). In section A–B note the flat topography at the O'a caldera due to the presence of Lake Shala. In panel (c) the red line with arrows indicates the lateral extent of the supposed GBVL on both margins. See text for further details. (For interpretation of the references to color in this figure legend, the reader is referred to the web version of this article.)

and not influencing the eastern plateau. These simple crustal-scale models were specifically designed to reproduce such a geometry at a scale of $\sim 5 \times 10^{-7}$ (1 cm in the experiment corresponded to ~20 km in nature; Fig. 5). The models were deformed in an artificial gravity field of ~18*g* using the large-capacity centrifuge available at the Tectonic Modelling Laboratory of the Institute of Geosciences and Earth Resources (National Research Council of Italy) and the Department of Earth-Sciences of the University of Florence. The models simulated a

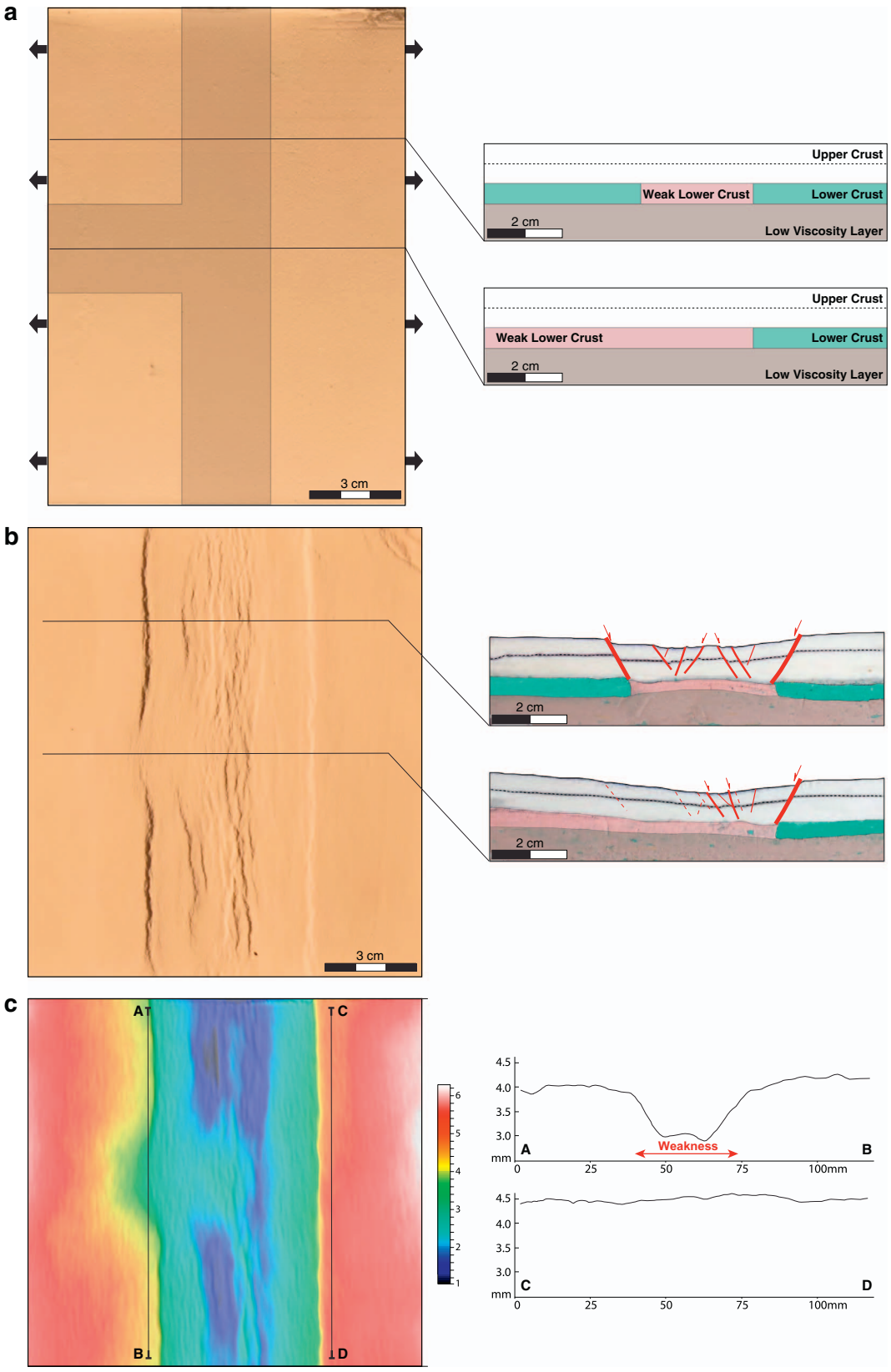

Fig. 5. (a) Top-view photo (left) and cross-sections (right) of the initial configuration of the analogue model. (b) Final top-view photo of the model (left) and cross-sections (right); note the strong asymmetry of the rift valley in the area interested by the transversal pre-existing weakness beneath the western plateau. (c) model surface topography obtained through laser scanning (left) and rift-parallel topographic profiles (right). Color scale in the left panel indicate topography in mm. Note the regular topography of the eastern margin that strongly contrasts with the topography of the western margin, which is characterized by a significant decrease in elevation of the plateau in the area corresponding to the transversal weakness. (For interpretation of the references to color in this figure legend, the reader is referred to the web version of this article.)

Table 2
Characteristics of experimental materials.

Prototype layer	Analogue material	Rheology	Thickness
Upper crust	K-feldspar powder	Brittle	10 mm (20 km)
Lower crust (normal)	Mixture of plasticine (Pongo Fantasia modelling dough, distributed by FILA) and PDMS-Polydimethylsiloxane (Dow Corning, SGM36) - 100:30% in weight	Ductile	5 mm (10 km)
Lower crust (weak)	Mixture of silicone (Dow Corning DC3179), corundum sand and oleic acid - 100:20:5% in weight	Ductile	5 mm (10 km)
Low viscosity layer	Mixture of DC3179, corundum sand and oleic acid - 100:80:15% in weight	Ductile	10 mm (20 km)

simplified rheological layering composed of brittle-ductile crust floating above a low viscosity material (Table 2). Similarly, the pre-existing weaknesses in our models represent a highly simplified version of inherited crustal fabrics in nature: for instance, they are modelled as pervasive fabrics in the lower crust only; the possible presence of inherited discrete brittle fabrics in the upper crust is not considered in our modelling.

It is beyond the scope of this modelling to analyse in detail the role of pre-existing heterogeneities on rift-related structures, as this aspect has been extensively in previous experimental works (e.g., Sokoutis et al., 2007 and references therein). The experiments of this study are tailored towards obtaining insights into the specific case under investigation.

4.2. Model results

Fig. 5 illustrates the results of an exemplificative model in which the preexisting transversal structure and the rift valley have the same width. The complete set of experiments, including additional models with a variable width of the preexisting transversal structure, is available open access in Corti et al. (2018b). Modelling results clearly illustrate the development of an extension-orthogonal rift valley bounded by major boundary fault systems, as commonly observed in similar experiments (e.g., Corti, 2012 and references therein). In particular, modelling results document the development of a rift valley bounded by major boundary fault systems localised along the pre-existing extension-orthogonal weakness. However, the transversal weakness beneath the western plateau had a prominent influence on the margin architecture. In particular, in agreement with what is observed in nature:

1) the large boundary faults are lacking in the area corresponding to the transversal weakness and the prominent marginal escarpment characterizing the western margin of the rift is in this area replaced by a gentle monocline with minor deformation only (Fig. 5). This also corresponds to a significant along-axis variation in rift structure. Model cross-sections display the typical symmetric nature of the rift basin characteristics of orthogonal rifting experiments. However, the lack of boundary faults and marginal escarpments in correspondence to the transverse weakness results in a locally strongly asymmetric architecture of the rift, with a gentle monocline on the western side and a major fault system on the eastern side (Fig. 5);

2) analysis of the model surface topography highlights a regular topography of the eastern margin, which strongly contrasts with the topography of the western margin. The latter is indeed characterized by a significant decrease in the plateau elevation in the area corresponding to the transversal weakness, where the marginal escarpment is lacking (Fig. 5).

Notably, both boundary and internal faults tend to be attracted by the transversal heterogeneity and to rotate to become oblique to extension (Fig. 5). Similar anomalous fault trends have been found in the rift floor northeast of Soddo (Corti et al., 2013a).

5. Geochemical characters of volcanic products

In order to provide additional constraints on the above-mentioned variations in structural and volcano-tectonic characteristics of the different sectors of the GBVL, an extensive sampling of recent volcanic products outcropping along this transversal structure has been carried out. In detail, 32 samples were selected for major and trace element geochemistry (data are shown in Supplementary Material Table SM1): from west to east, 5 are from the Tepi volcanic field, 6 from the Wagebeta caldera complex on the western shoulder of the MER, 10 from the Soddo area and the Awasa and Corbetti calderas in the axial portion of the MER, 3 from scattered volcanic centres around Dodola, on the eastern side of the lineament, and 8 from the Bale Mountains, at the eastern end (Figs. 2, 3).

5.1. Methods

Rock samples were cut with a diamond-disc saw and ground in a steel mill. The grits were washed with distilled water, dried overnight in an oven at 60 °C, and pulverized in a low-blank agate mortar. Whole-rock major and trace element analyses were determined by ICP-AES (Inductively Coupled Plasma-Atomic Emission Spectrometry) and ICP-MS (Inductively Coupled Plasma-Mass Spectrometry), respectively, at Actlabs (Ontario, Canada), after lithium metaborate and lithium tetraborate fusion, according to the 4LITHO code. Analytical precision for trace elements is generally better than 5%. Trace Elements for samples SE11, SE12 determined via XRF at Dipartimento di Scienze della Terra, Università di Pisa on Li-metaborate and Li-tetraborate fused glass discs. Accuracy is between 3 and 10%.

The data from this geochemical analysis are plotted along with existing literature data from Tepi (Ayalew et al., 2002), Wagebeta on the western side (WoldeGabriel et al., 1990), Corbetti and Aluto calderas in the rift (Hutchison et al., 2016; Rapprich et al., 2016), and from the Chilalo volcanic centre (Trua et al., 1999) on the eastern shoulder of the rift, as described in the following sections.

5.2. Results: major and trace elements

On the TAS, Total Alkali vs. Silica, classification diagram, the samples from both Tepi and Bale, as well as those on western and eastern side of the lineament (Fig. 6), belong to a mildly alkaline association showing a bimodal distribution with a Daly Gap (Daly, 1925), typical of the MER volcanism as well as most of continental rift volcanism worldwide (e.g. Clague, 1978 and references therein). Samples mainly fall inside the basalt, trachy-basalt and basaltic trachyandesite fields, on the one side, and trachyte and rhyolite fields, on the other side. Only four samples belong to the intermediate rocks (three are from Chilalo, and one from Soddo area).

Harker diagrams (Fig. 7) depict the evolutionary paths of the studied rocks. MgO, Cao, FeO and TiO_2 exhibit typical negative correlation with silica content: in more detail, it is noteworthy that MgO decreases

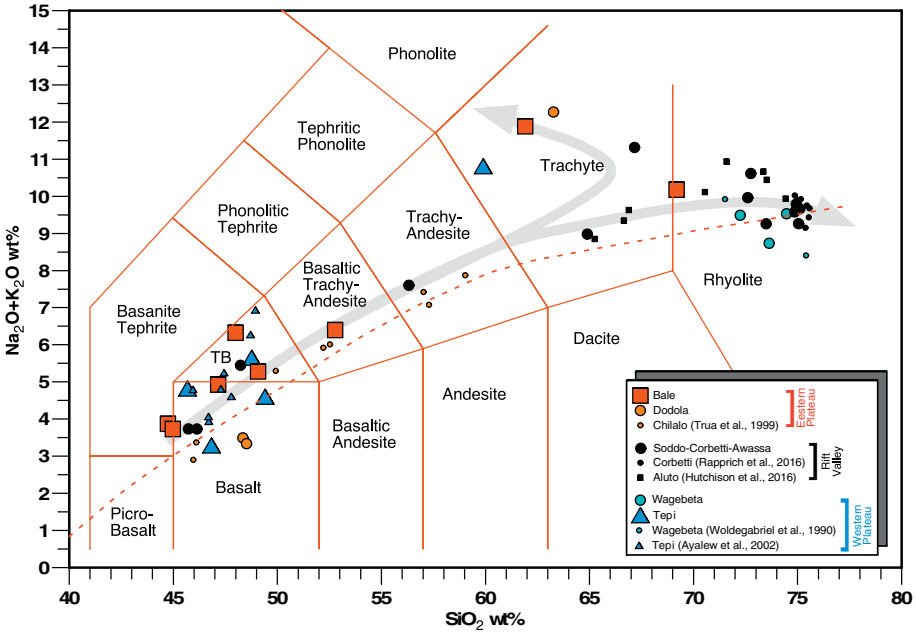

Fig. 6. TAS (Total Alkali vs. Silica) classification diagram of volcanic rocks along the Goba-Bonga lineament. Field after Le Bas et al. (1986). Line dividing alkaline and subalkaline field from Irvine and Baragar (1971). TB, trachybasalts. Grey arrows indicate the two possible evolution patterns (see text for details).

abruptly during the first step of evolution, whereas CaO show a change in slope. The Al_2O_3 vs SiO_2 diagram is characterized by a humped pattern, with a clear increase during the first steps of evolution, then a negative slope. Fundamental constraints on petrologic evolution of studied rocks derive from the observation of these trends: these samples evolved mainly by crystal fractionation with fractionation assemblages varying significantly for basaltic and evolved rocks. Basaltic rocks *sensu latu* (SiO_2 = 43–55%) evolve by removal of femic phases, such as olivine and clinopyroxene, along with Fe—Ti oxides, whereas Al-rich phases such as plagioclase have a negligible role. On the contrary, feldspar fractionation controls the successive stages of evolution: removal of Ca-plagioclase dominates the intermediate steps (trachy-andesites to trachytes). Then, after CaO fall to very low values at SiO_2 = 65%, Na-rich alkali feldspar (anorthose) and albitic plagioclase, became the major fractionating phases, as evidenced by the constant (or slightly increasing) K_2O and from the Na_2O decrease depicted by rhyolite samples.

In addition, when paying more attention to the most evolved rocks, from the TAS diagram, as well as from Na_2O and K_2O trends in Fig. 7, we notice that two distinct evolutionary paths were followed during the second stage of crystallization: the first, depicted by most samples, shows a continuous increase of SiO_2 and K_2O, and a final decrease in Na_2O, leading to the aforementioned alkali-rhyolites and rhyolites as the most evolved products. The second evolutionary path is characterized by a SiO_2 decrease during the latest stage of evolution, pointing towards the peralkaline series, and evolved trachytes are its latest products. This double trend in the late stage of evolution is clearly visible in most Harker diagrams (e.g. all elements but Al_2O_3 and MgO, see grey arrows in Fig. 7), and is epitomised by the trends in Fig. 8, where K and Differentiation Index (DI) are plotted against Na_2O. DI is calculated by summing the normative Quartz, Albite, Orthose and Nepheline. The K_2O/Na_2O ratio increases with increasing degree of evolution, whereas Na_2O content may follow two paths: evolution to SiO_2-oversaturated rhyolitic melts, or evolution to SiO_2-undersaturated trachytic melts. This evolution is quite typical in alkaline series evolving via crystal fractionation: the fractionation assemblage is dominated by plagioclase and alkali feldspar with a chemical composition very close to that of the melt; if the melt is slightly higher in SiO_2 and lower in Na_2O than the fractionating phases, their removal will lead to the oversaturated trend and rhyolite will form. In the case that the melt is lower in SiO_2 and higher in Na_2O with respect to fractionating phases, the undersaturated pathway will be followed.

Regarding the geographical and geological context of the samples, in the western side we found mostly basaltic rocks, but a SiO_2 - undersaturated trachyte in Tepi, and SiO_2 - oversaturated rhyolites at the Wagebeta complex. Here, intermediate products are completely lacking. The volcanism in the axial zone of the rift exhibits a Daly Gap, with rhyolitic products more abundant in Soddo, and exclusive at Corbetti and Aluto. To the east, we found a continuous evolutionary trend at Dodola-Chilalo, without Daly Gap (e.g., Trua et al., 1999), and without evolved products (except one sample), and bimodal volcanism at Bale Mountains.

The distribution of incompatible trace elements, normalized to Primitive Mantle (PM; McDonough and Sun, 1995), is shown in the spider diagrams presented in Fig. 9. Basic samples from different locations show very similar characteristics, including fractionated patterns and a general positive anomaly in Nb and Ta. Pb is below the detection limit in many samples and a negative Pb spike is reported in the remainder. Evolved rocks have similar patterns with respect to the basic rocks, with highest levels of the most incompatible elements, such as Rb, Th and U, besides Nb and Ta, and with strong negative anomalies of Ba, Sr, P and Ti.

Rare Earth Elements (REEs) for basic samples, normalized to CI Chondrite, are quite fractionated and mostly linear with the slope declining for heavy REEs and small negative Eu anomalies. Evolved samples show almost flat heavy REE patterns.

5.3. Geochemical constraints on magmatic activity

Spider diagrams of basic rocks are a powerful tool to infer information on the characteristics of the mantle source, whereas spider diagrams of evolved rocks may also provide information on evolutionary processes. No substantial differences are found for both basic and acid samples, in the spider diagrams for samples collected east or west from the axial valley. This indicates that the mantle source sampled by these magmas is very similar. The entire dataset show humped patterns (Fig. 9), marked by a peak at Nb—Ta, indicative of a mantle asthenosphere source unaffected by any subduction imprint. The

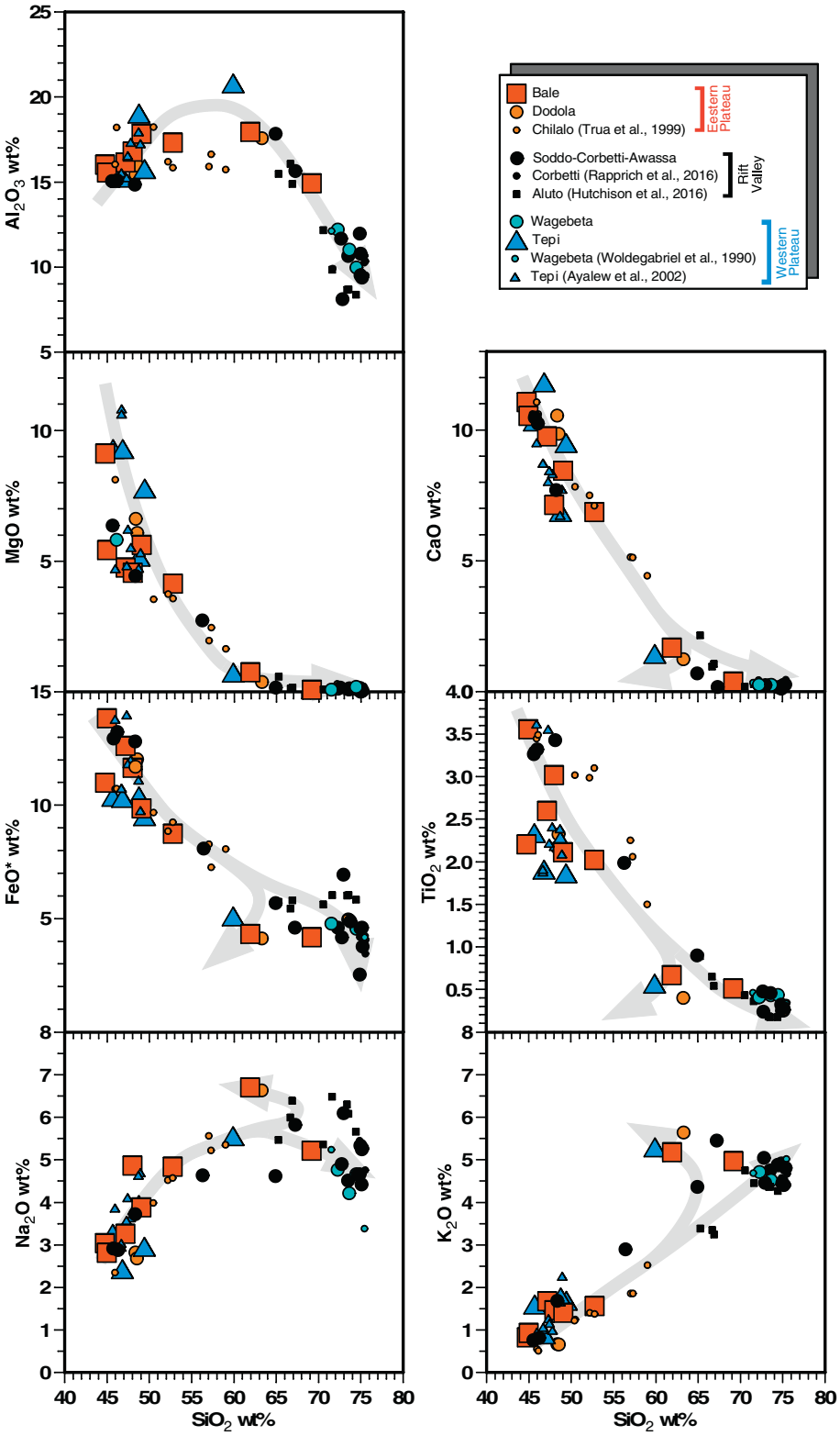

Fig. 7. Major elements vs. SiO_2 (wt% recalculated on a LOI-free basis) diagrams of volcanic rocks along the Goba-Bonga lineament. Grey arrows indicate the two possible evolution patterns.

similar slopes of spider diagrams for all of the trace elements, and the lack of strong heavy REE (Rare Earth Element) fractionation point out that partial melting occurred at similar depths, in the spinel peridotite stability field, that is at depth < 60–80 km. Indeed, melting of garnet bearing peridotites partial melting usually produce a steep HREE pattern, which is not observed for the REE diagrams of Fig. 9.

The negative Ba, Sr, P and Ti anomalies observed in intermediate-acidic rocks are not due to the source characteristics but depend on removal of fractionating phases during the evolution of the magma, namely plagioclase (Ba and Sr), apatite (P), and oxides (Ti). The occurrence of plagioclase removal is confirmed by the negative Eu anomaly in the REE pattern. The observed flat trend for the medium-

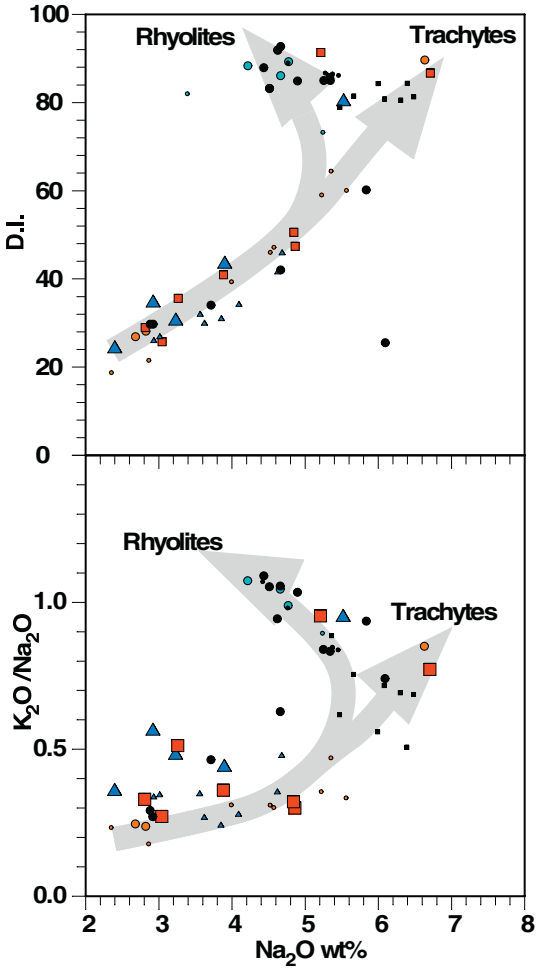

Fig. 8. K2O/Na2O and Differentiation Index vs. Na2O diagrams of volcanic rocks along the Goba-Boga lineament. Symbols as in Fig. 7.

heavy REEs may be explained by contemporaneous fractionation of a mineral in which these elements are partially compatible, like clinopyroxene. These data are in fully agreement with the observations gained from major element variations.

To better investigate mantle source of magmas, studied samples are plotted in Ta/Yb vs. Th/Yb diagram (Fig. 10): all of them plot along the so-called mantle array, close to OIB (Ocean Island Basalt) field. Some of the more evolved samples have higher Th/Yb values, with a limited shift towards values of the Upper Continental Crustal, indicating a contribution from crustal assimilation during magma evolution. Primitive samples from the Bale area have lower Th/Yb and Ta/Yb ratios, along with samples from the Dodola and Chilalo areas, also on the eastern side of the rift. Part of the Tepi basalts, located in the western end of the lineament, have similar Th/Yb and Ta/Yb ratios with respect to the other samples. However, especially new data on more primitive Tepi products, cluster on the upper right-hand-side of the diagram (higher Yh/Yb and Ta/Yb ratios, Fig.10). These differences may be due to different source depletion, or different partial melting degree. Given the relative homogeneity of mantle source, our preferred interpretation is that the most relevant difference between Bale Mountains and Tepi volcanic field is the melting degree, which is higher at Bale and lower at Tepi.

In addition, the Tepi samples display other two significant differences among the studied datasets: (i) no Eu-negative anomaly, even in the only evolved trachytic sample; (ii) lower Zr and Hf contents than samples from Bale Mts. or the axial rift. The absence of Eu negative anomaly points out that plagioclase was virtually absent from the at Tepi, the fractionating assemblage during magma evolution; this observation is also in fully agreement with the fact that the evolved sample of Tepi do not display any Al_2O_3 removal in Fig. 7, being on the contrary the sample with the highest Al_2O_3 content of the whole dataset. The Hf and Zr enrichments are usually indicative of upper crustal contamination, mainly due to magma evolution in upper crustal shallow chamber. These two peculiar characters of Tepi volcanics, both indicate that Tepi magmas reached the surface easier and faster than samples from axial rift or eastern part.

6. Discussion

6.1. Characteristics of the Goba-Bonga volcano-tectonic lineament

Our analysis support that the major, roughly E–W-trending Goba-Bonga volcano-tectonic lineament is characterized by occurrence of prominent, recent tectonic and volcanic activity affecting the Ethiopian plateau up to ~300 km to the west of the MER (Fig. 11). In particular, our structural analysis confirms the existence of two different fault trends: the ENE–WSW-trending Tepi fault, and the ESE–WNW-trending Gojeb graben (or Bonga fault; e.g., Berhe et al., 1987). The volcanic activity at Tepi is strictly controlled by structural features, resulting in an overall alignment of volcanic vents trending sub-parallel with faults affecting the area. Although the timing of fault activity is difficult to constrain, the observation that the majority of the faults do not affect the most recent (Pleistocene) volcanic deposits indicates a decrease in tectonic activity after the Pliocene. However, a prominent morphotectonic signature points to a recent activity at least for some faults. Fault slip data and the alignment of volcanic vents at Tepi are consistent with a roughly NNW-SSE extension, which is about orthogonal to the current WNW-ESE-trending regional extension direction. Similarly, the recent activity of the ESE–WNW-trending faults bounding the Gojeb graben is difficult to reconcile with the current Nubia-Somalia motion. Previous works (e.g., Bonini et al., 2005) suggested that these faults formed during Oligocene times in response to extensional stresses related to Africa-Arabia separation; these structures may have been later reactivated during Pliocene-Recent rifting. The extensional stress field responsible for this reactivation and for the volcano-tectonic activity in the Tepi area may have been controlled by recent episodes of uplift of the Ethiopian plateau (Gani et al., 2007). Lithospheric uplift has been indeed shown to represent an efficient source of extensional stresses, able to lead to the reactivation of pre-existing structures and to exert a control on the alignments of volcanic vents, as suggested for instance in the French Massif Central (Michon and Merle, 2001). Local reorientation of the extension direction by inherited basement fabrics may have contributed to the almost N—S extension on the roughly E–W faults in the western plateau (e.g., Morley, 2010; Corti et al., 2013b; Philippon et al., 2015).

Within the rift floor, the E–W alignment of Awasa and Corbetti calderas has been likely controlled by the Goba-Bonga fabric, as suggested by previous studies (Acocella et al., 2002). Conversely, no tectonic nor volcanic features that can be associated with a roughly E–W structure have been recognized on the eastern plateau. Indeed, although the volcanic centres of Chike, Kaka and Hunkuolo may resemble an approximately E–W alignment (see above Section 3.3), our analysis of distribution of volcanic centres on the Somalian Plateau indicates preferential elongation in a roughly NNE-SSW direction (e.g., Mohr and Potter, 1976; Wolde, 1989). The rift margin east of Lake Langano curves to acquire a local NW-SE trend, suggesting a control exerted by a transversal pre-existing structure (e.g., Corti, 2009 and references therein). The NW-SE orientation suggests that this inherited structure is unrelated to the GBVL; rather, the margin has been more likely controlled by another, pre-existing structure now evidenced by gravity data as a NW-SE graben buried below the rift depression and filled with low-density sediments (Korme et al., 2004).

At the latitude of the GBVL, the western rift margin displays atypical

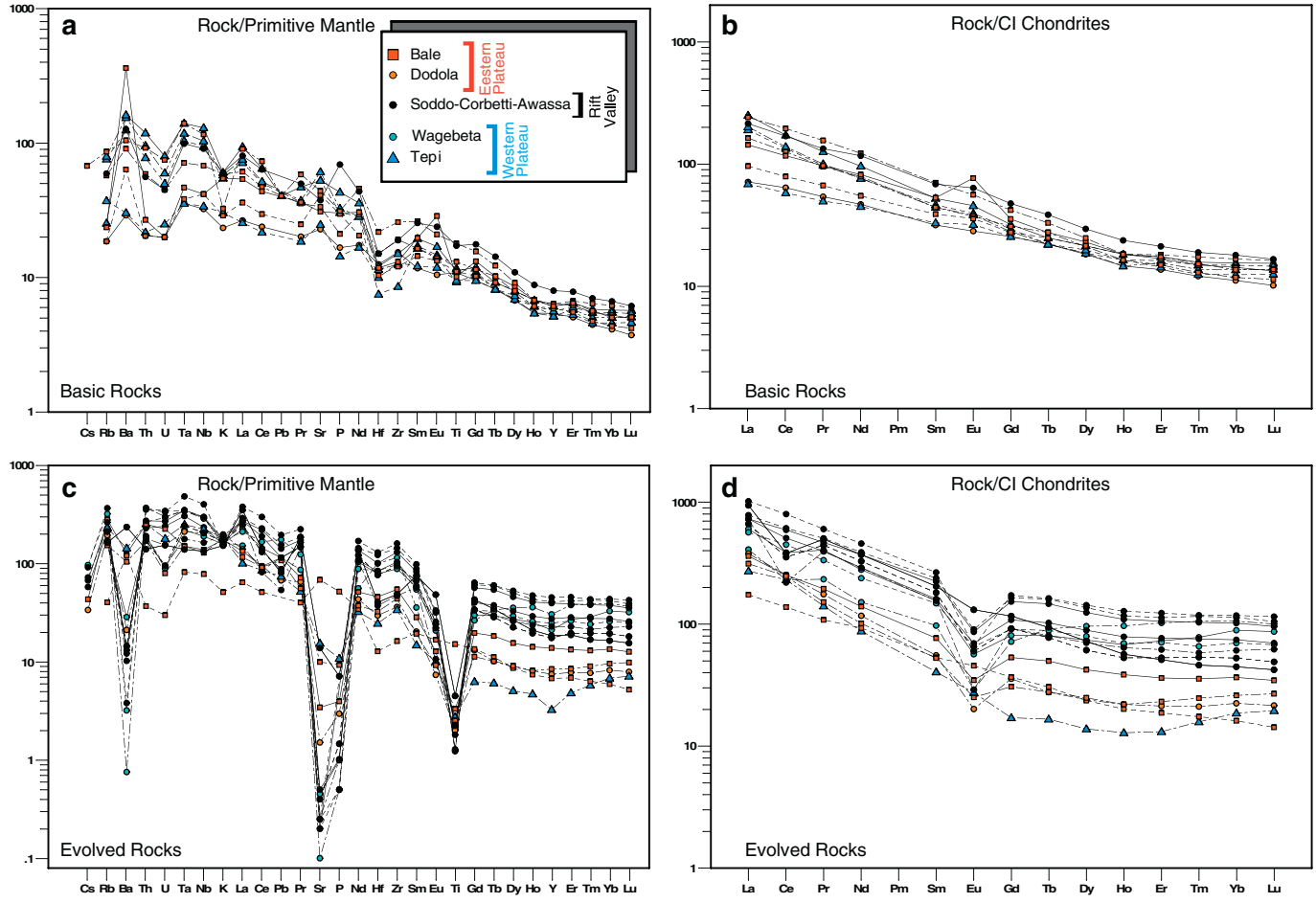

Fig. 9. Multi-elemental trace element variation patterns for Primitive Mantle-normalized incompatible trace element (left) and Chondrite-normalized Rare Earth Element (right) of basic and evolved rocks of the study area. Normalizing values after McDonough and Sun (1995).

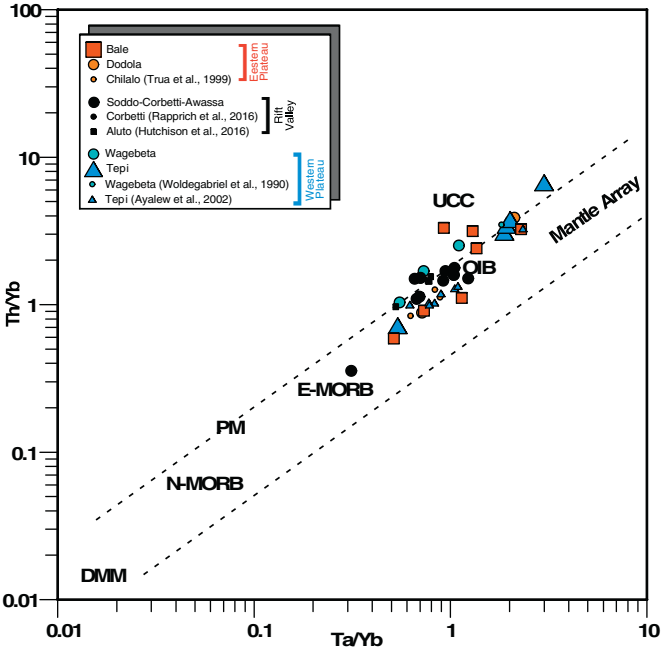

Fig. 10. Th/Yb vs Ta/Yb diagram for the volcanic rocks of the study area. UCC: Upper Continental Crust; DMM: Depleted MORB Mantle; E-MORB: Enriched Mid Ocean Ridge Basalts; N-MORB: Normal Mid Ocean Ridge Basalts; OIB: Oceanic Islands basalts; PM: Primitive mantle. Fields as reported in Pearce (1982).

structure (i.e., absence of a major boundary fault) and morphology (i.e., anomalous low elevation with respect to surrounding sectors), whereas the eastern margin is characterized by negligible lateral variations and displays major boundary faults and elevated topography. This results in an asymmetric rift structure at the latitude of the GBVL, which contrasts with more symmetric structure to the north and south of this lineament. These differences in topography and architecture in the Soddo region (i.e., the area supposedly intersected by the GBVL) could be controlled by magma intrusion and related heating/weakening. These processes are in fact able to reduce the thickness of the brittle crust resulting in rift-related deformation accommodated by dense swarms of small normal faults with limited vertical offset (e.g., Ebinger et al., 1999), as observed in the axial Northern MER (Corti, 2009 and references therein). However, magmatism cannot represent the only driving process for the observed difference in margin architecture, since it is voluminous in other areas (e.g., Guraghe) where the margin is characterized by a major escarpment with a few, major boundary faults. Similarly, the variation in margin morphology and fault pattern cannot be controlled by changes in lithology, since the whole Guraghe-Fonko-Soddo margin is depicted by a similar stratigraphy with plateau basalts, overlaid by widespread Pliocene ignimbrites and Quaternary bimodal volcanites and volcano-sedimentary deposits (e.g., Corti et al., 2013a). Extrapolation of analogue modelling results indicate instead that this variation could be controlled by the presence of the E–W trending pre-existing crustal/lithospheric anisotropy, which causes the boundary faults to be replaced by a gentle monocline (and minor normal faults) resulting in a locally lower topography with respect to the adjoining margin sectors.

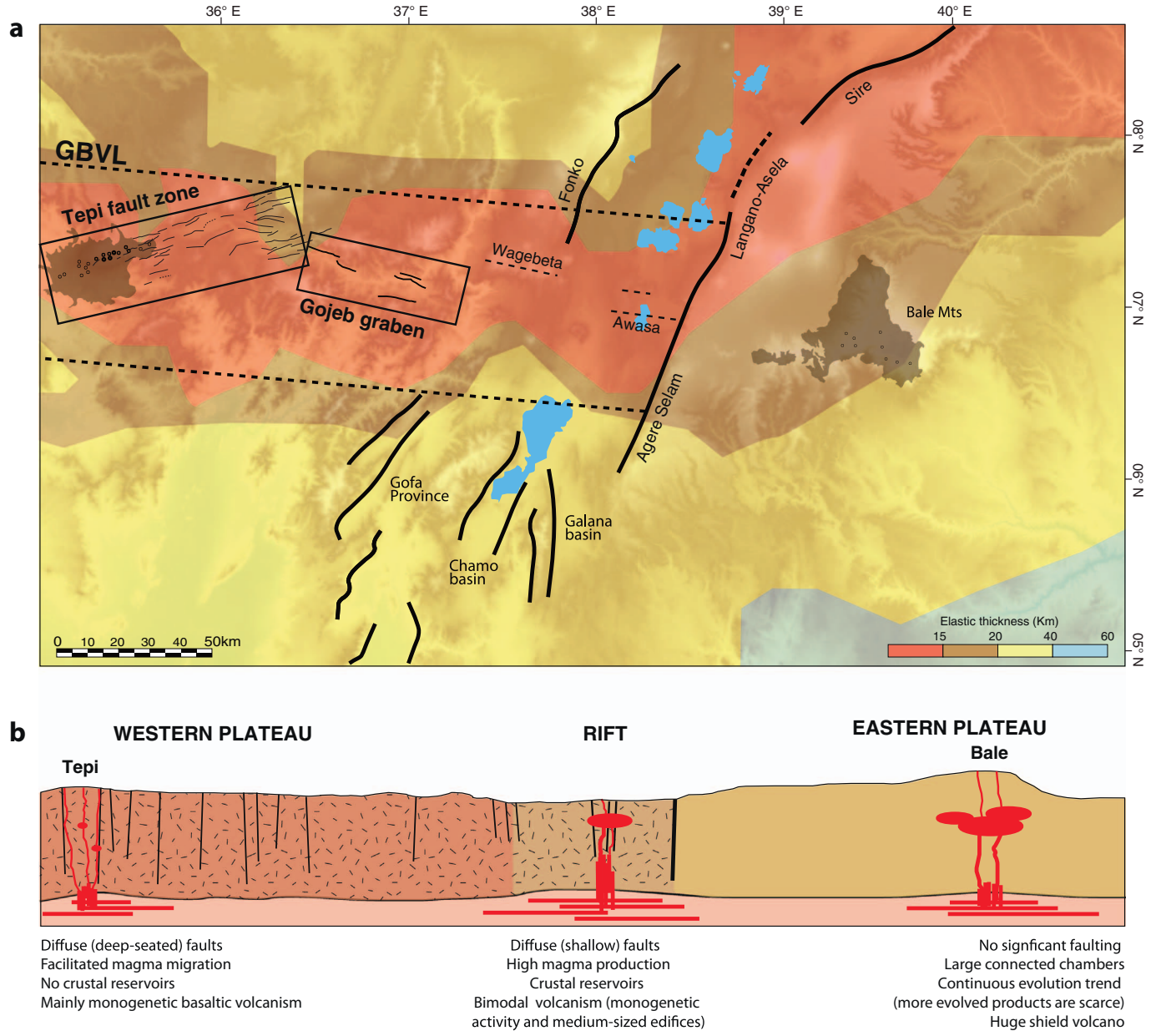

Fig. 11. a) Summary structural scheme of the Goba Bonga lineament, superimposed on a map of the elastic thickness of the lithosphere after Pérez-Gussinyé et al. (2009). Note the low values (Te < 10–15 km) in a narrow region extending in a roughly E–W direction between Tepi and the rift valley, in the region corresponding to the extent of the GBVL. Also note the higher values beneath the eastern plateau, where Te can reach values >40 km. b) Schematic cross-section summarizing the main characteristics of the volcano-tectonic activity in the Western and Eastern plateaus and in the rift valley.

6.2. *The Goba-Bonga volcanic rocks: tectonic implications*

The geochemical characters of volcanic rocks are quite similar throughout the entire extension of the Goba-Bonga volcano-tectonic lineament, from the Tepi volcanic field to the Bale Mountains. Both west and east of the rift, scattered basaltic products (*sensu latu*) generated from very similar source, i.e. spinel peridotite unaffected by any subduction imprint, subjected to partial melting at similar pressure (and depth). Evolved products formed by fractional crystallization, matched by small amount of crustal contamination, in shallow upper crustal magma chambers. The limited observed differences, both for major and trace elements may be explained with minor source heterogeneities, and/or with some differences in melting degree. Given the relative homogeneity of mantle source, our preferred interpretation is that the most relevant difference between the Tepi volcanic field and the Bale Mountains is the melting degree, which is higher at Bale and lower at Tepi. This is also confirmed by the volume of erupted products, which is very small at Tepi (only a few 100-300 m-high monogenetic cones), and very impressive at Bale (a huge shield volcano, some 70–80 km in diameter and rising >2000 m from the plateau).

In addition, the distribution of volcanic activity as a function of the geographical and geological context retains significant heterogeneity: bimodal volcanism with mainly basaltic products to the west, bimodal volcanism with mainly rhyolitic products in the axial rift, continuous evolution from basalt to trachy-andesite and very rare evolved products to the east.

Then, we can conclude that at Tepi the predominance of basaltic products, along with the lacking of evidences for residence in shallow reservoirs, witness for the ease at which magma is able to migrate to the surface due to well-developed fault system.

Differently from Tepi, in the western part of the GBVL, at the Wagebeta complex and in the axial zone of the rift some basaltic

magmas reach the surface directly, but most of them reside in shallow magma chambers, and evolve with significant amount of plagioclase removal, mostly to rhyolites. If geochemical evolution is similar, magma production is much higher in the axial zone of the rift. Here, extensional dynamics lead to formation of upper crustal magma chambers, which in turn affected crustal dynamics and fault patterns.

A different magma evolution is observed when considering volcanic products found in the eastern plateau: here no Daly Gap is observed, and more evolved products are scarce, suggesting that the magmas once formed, their ascent was likely driven by deep-seated pre-existing discontinuities, started to differentiate during their upraise and then eventually collected in larger connected magma chambers. In this frame, whereas on the western side of the GBVL, as well as in the axial valley, magmas were diffusely drained, with lot of monogenetic cones, and some medium-sized edifices, in the eastern side magmatic activity is quite limited in the internal part, and in external part is gathered in a huge shield-volcano.

6.3. Role of the inherited lithospheric structure on the transversal volcano-tectonic lineaments

In summary, we observe three different kinds of tectono-magmatic evolution from west to east: (1) in the western plateau, the diffuse fault network likely reactivating deep-seated pre-existing structures allowed most of the magmas to reach the surface without differentiation and volcanism is mainly monogenetic. (2) In the axial rift valley, faults affect a thermally modified lithosphere; in these conditions shallower faults and large-scale magma production led to bimodal activity, characterized by basaltic, monogenetic scoria cones and lava flows on the one hand, and trachytic-rhyolitic pyroclastic products and lava domes on the other, as previously observed by many Authors (e.g., WoldeGabriel et al., 1990). (3) In the eastern plateau, faults are limited or absent, and we observe a continuous evolution trend, with low abundance of evolved products, pointing out for a magma collection in larger magma chambers, and allowing the formation of larger volcanic edifices, like the impressive shield volcano of Bale Mountains.

All these observations suggest that the volcano-tectonic features associated with the GBVL affect the western plateau and the rift floor only; extrapolation of analogue modelling suggests that this pattern has been likely controlled by the presence of a roughly E–W pre-existing discontinuity beneath the Ethiopian plateau not extending beneath the eastern plateau (Fig. 11). This likely results from the different characteristics of the lithosphere beneath the western and eastern plateaus (Corti et al., 2018a). Geophysical data suggest indeed a striking contrast between the heterogeneous, weak Ethiopian plateau south of the YTVL and the more uniform, stronger Somalian plateau (e.g., Keranen and Klemperer, 2008; Keranen et al., 2009). This eastern plateau acts as a strong block not characterized by significant pre-existing heterogeneities (e.g., Corti et al., 2018a). The existence of roughly E–W pre-existing discontinuity beneath the western plateau is supported by analysis of the elastic thickness (Te) of the lithosphere (Pérez-Gussinyé et al., 2009), which indicates low values (Te < 10–15 km) in a narrow region extending in a roughly E–W direction between Tepi and the rift valley (Fig. 11). Conversely, the elastic thickness of the lithosphere is much higher beneath the eastern plateau, where Te can reach values > 60 km, supporting its stronger, more uniform rheology (Fig. 11). The pre-existing nature of the GBVL is also supported by the significant crustal thinning south of this lineament (e.g., Woldetinsae and Götze, 2005; Keranen and Klemperer, 2008) and by the control exerted by this structure on the northward propagation of the Kenya rift-related deformation at ca. 20 Ma (Bonini et al., 2005; Philippon et al., 2014; Balestrieri et al., 2016).

The pattern of deformation described above for the GBVL is strikingly similar to that described for the YTVL, which is interpreted to represent a pre-existing weakness zone, sub-parallel to the trend of the Gulf of Aden, characterizing the Ethiopian plateau and not extending into the eastern plateau (e.g., Abebe et al., 1998; Korme et al., 2004; Corti et al., 2018a). Notably, the presence of these pre-existing transversal structures on the western plateau interrupts the lateral continuity of major boundary faults on the western margin, which are replaced by gentle monoclines dipping towards the rift axis. This, together with a more continuous border fault system on the eastern margin (related to the presence of a strong lithosphere beneath the Somalian plateau) results in a marked rift asymmetry at the latitude of both the GBVL and YTVL (Corti et al., 2018a, 2018b).

These observations support the importance of the heterogeneous nature of the lithosphere and the spatial variations in its structure in controlling the architecture of continental rifts and the distribution of the related volcano-tectonic activity (e.g., Ziegler and Cloetingh, 2004; Sokoutis et al., 2007; Corti, 2012; Laó-Dávila et al., 2015; Brune, 2016; Corti et al., 2018a). In particular, the different degree of faulting in the western and eastern plateau, associated with different geochemical characteristics of volcanic rocks despite a similar mantle source, may reflect a different vertical extent of the pre-existing fabrics affecting the Ethiopian lithosphere. Previous modelling (Sokoutis et al., 2007) has shown that the pattern and characteristics of the extension-related deformation is largely influenced by vertical distribution of pre-existing weaknesses (e.g., if they affect the lithospheric mantle and/or the crust), with more prominent faulting when the inherited heterogeneity affects the whole lithosphere. Therefore, one possibility is that the transversal pre-existing fabric may affect the whole lithosphere beneath the western plateau (enhanced faulting and easier magma migration) and only the mantle beneath the eastern plateau (absent upper-crustal deformation and more difficult magma upraising).

7. Conclusions

We have conducted new remote and field-based structural analysis, coupled with a new series of analogue models, and new geochemical analyses to improve the knowledge of the Goba-Bonga volcano-tectonic lineament, which represents one of the most important transverse structures in the Main Ethiopian Rift. The integrated analysis suggests the following conclusions:

1. The major, roughly E–W-trending Goba-Bonga lineament is characterized by prominent volcano-tectonic activity affecting the Ethiopian plateau, with structures reflecting two different fault systems: the ENE–WSW-tending Tepi fault, and the ESE–WNW-trending Gojeb graben. Within the rift floor, the approximately E–W alignment of Awasa and Corbetti calderas likely represents an expression of the Goba-Bonga. Conversely, no tectonic or volcanic features that can be associated with a roughly E–W structure have been recognized on the eastern plateau.
2. Major variations in the structure (i.e., absence of a major boundary fault) and topography (i.e., anomalous low elevation with respect to surrounding sectors) of the western rift margin are observed at the latitude of the Goba-Bonga lineament; the eastern margin is instead more uniform and lacks significant lateral variations. This results in significant along-axis changes in rift structure, which is asymmetric at the latitude of the Goba-Bonga structure, and more symmetric to the north and south of this lineament.
3. Comparison between these observations and analogue modelling suggests that the volcano-tectonic features of the Goba-Bonga lineament have been likely controlled by the presence of a roughly E–W pre-existing discontinuity beneath the Ethiopian plateau not extending beneath the eastern plateau.
4. The geochemistry of volcanic rocks supports this interpretation and indicate that, although magmas have the same sub-lithospheric mantle source (with partial melting at same depths and minor source heterogeneities, and with some differences in melting degree), limited differences in magma evolution witnesses for different tectonic framework to the west, to the east, and in the axial zone of

the rift. Specifically, diffuse deep-seated faulting able to drain magmas and forming monogenetic cones characterizes the Tepi region; diffuse shallow faulting and magma collecting in shallow upper crustal chambers characterize the rift valley in the Soddo area; magma gathering to form a large shield volcano is the dominant feature in the poorly faulted eastern portion of GBVL, at the Bale Mountains.

Supplementary data to this article can be found online at https://doi.org/10.1016/j.tecto.2018.02.011.

Acknowledgments

We thank Laurent Michon and one anonymous Reviewer for the fruitful comments that helped to improve the manuscript. We also thank Daniele Maestrelli for the swath profiles reported in Fig. 4. M. Philippon, D. Sokoutis, E. Willingshofer acknowledge the financial support from the Marie Curie Initial Training Network TOPOMOD project 264517. G. Corti and F. Sani acknowledge the financial support from MIUR project (PRIN2009 - prot.2009H37M59). Inversion of fault-slip data and volcanic alignments was obtained using Win-Tensor, a software developed by Dr. Damien Delvaux, Royal Museum for Central Africa, Tervuren, Belgium.

References

Abbate, E., Sagri, M., 1980. Volcanites of Ethiopian and Somali plateaus and major tectonic lines. Atti Convegni Lincei 47, 219–227.
Abbate, E., Bruni, P., Sagri, M., 2015. Geology of Ethiopia: a review and geomorphological perspectives. In: Billi, P. (Ed.), Landscapes and Landforms of Ethiopia, World Geomorphological Landscapes. Springer Science + Business Media, Dordrecht, pp. 33–64.
Abebe Adhana, T., 2014. The occurrence of a complete continental rift type of volcanic rocks suite along the Yerer–Tullu Wellel volcano tectonic lineament, Central Ethiopia. J. Afr. Earth Sci. 99, 374–385.
Abebe, T., Mazzarini, F., Innocenti, F., Manetti, P., 1998. The Yerer - Tullu Wellel Volcanotectonic lineament: a transtentional structure in Central Ethiopia and the associated magmatic activity. J. Afr. Earth Sci. 26, 135–150.
Acocella, V., Korme, T., Salvini, F., Funiciello, R., 2002. Elliptic calderas in the Ethiopian rift: control of pre-existing structures. J. Volcanol. Geotherm. Res. 2512, 1–15.
Agostini, A., Bonini, M., Corti, G., Sani, F., Mazzarini, F., 2011. Fault architecture in the main Ethiopian rift and comparison with experimental models: implications for rift evolution and Nubia-Somalia kinematics. Earth Planet. Sci. Lett. 301, 479–492.
Ayalew, D., Barbey, P., Marty, B., Reisberg, L., Yirgu, G., Pik, R., 2002. Source, genesis and timing of giant ignimbrite deposits associated with Ethiopian continental flood basalts. Geochim. Cosmochim. Acta 66, 1429–1448.
Ayalew, D., Marty, B., Barbey, P., Yirgu, G., Ketefo, E., 2006. Sub-lithospheric source for Quaternary alkaline Tepi shield, southwest Ethiopia. Geochem. J. 40, 47–56.
Balestrieri, M.L., Bonini, M., Corti, G., Sani, F., Philippon, M., 2016. A refinement of the chronology of rift-related faulting in the broadly rifted zone, southern Ethiopia, through apatite fission-track analysis. Tectonophysics 671, 42–55. http://dx.doi.org/10.1016/j.tecto.2016.01.012.
Bellahsen, N., Daniel, J.M., 2005. Fault reactivation control on normal fault growth: an experimental study. J. Struct. Geol. 27, 769–780.
Berhe, S.M., Desta, B., Nicoletti, M., Teferra, M., 1987. Geology, geochronology and geodynamic implications of the Cenozoic magmatic province in W and SE Ethiopia. J. Geol. Soc. Lond. 144, 213–226.
Bonini, M., Corti, G., Innocenti, F., Manetti, P., Mazzarini, F., Abebe, T., Pecskay, Z., 2005. Evolution of the main Ethiopian rift in the frame of Afar and Kenya rifts propagation. Tectonics 24 (1), TC1007. http://dx.doi.org/10.1029/2004TC001680.
Brune, S., 2016. Rifts and rifted margins: a review of geodynamic processes and natural hazards, edited by J. C. Duarte and W. P. Schellart, Plate Boundaries. Nat. Hazards 11–37. http://dx.doi.org/10.1002/9781119054146.ch2.
Clague, D.A., 1978. The oceanic basalt-trachyte association: an explanation of the Daly Gap. J. Geol. 86, 739–743.
Corti, G., 2009. Continental rift evolution: from rift initiation to incipient break-up in the main Ethiopian rift, East Africa. Earth-Sci. Rev. 96, 1–53.
Corti, G., 2012. Evolution and characteristics of continental rifting: analogue modeling-inspired view and comparison with examples from the east African rift system. Tectonophysics 522-523, 1–33.
Corti, G., van Wijk, J., Cloetingh, S., Morley, C.K., 2007. Tectonic inheritance and continental rift architecture: numerical and analogue models of the east African rift system. Tectonics 26, TC6006. http://dx.doi.org/10.1029/2006TC002086.
Corti, G., Sani, F., Philippon, M., Sokoutis, D., Willingshofer, E., Molin, P., 2013a. Quaternary volcano-tectonic activity in the Soddo region, western margin of the southern main Ethiopian rift. Tectonics 32, 861–879.
Corti, G., Philippon, M., Sani, F., Keir, D., Kidane, T., 2013b. Re-orientation of the extension direction and pure extensional faulting at oblique rift margins: comparison between the main Ethiopian rift and laboratory experiments. Terra Nova 25, 396–404.
Corti, G., Molin, P., Sembroni, A., Bastow, I.D., Keir, D., 2018a. Control of pre-rift lithospheric structure on the architecture and evolution of continental rifts: insights from the Main Ethiopian Rift, East Africa. Tectonics 37. http://dx.doi.org/10.1002/2017TC004799.
Corti, G., Sordi, R., Cucci, F., 2018b. Centrifuge models investigating the influence of transverse pre-existing weaknesses on continental rifting. GFZ Data Services. http://dx.doi.org/10.5880/fidgeo.2018.001.
Daly, R.A., 1925. The geology of Ascension Island. Proc. Am. Acad. Arts Sci. 60, 3–80.
Davidson, A., 1983. The Omo River project: reconnaissance geology and geochemistry of parts of Illubabor, Kefa, Gemu Gofa, and Sidamo. Ethiopian Inst. Geol. Surv. Bull. 2, 1–89 (compiler).
Delvaux, D., Sperner, B., 2003. Stress tensor inversion from fault kinematic indicators and focal mechanism data: the TENSOR program. In: Nieuwland, D. (Ed.), New Insights into Structural Interpretation and Modelling. 212. pp. 75–100 Geological Society, London, Special Publications.
Ebinger, C., 2005. Continental breakup: the east African perspective. Astron. Geophys. 46, 2.16–2.21.
Ebinger, C.J., Jackson, J.A., Foster, A.N., Hayward, N.J., 1999. Extensional basin geometry and the elastic lithosphere. Philos. Trans. R. Soc. Lond. Ser. Math. Phys. Eng. Sci. 357 (1753), 741–765. http://dx.doi.org/10.1098/rsta.1999.0351.
Faulds, J.E., Varga, R.J., 1998. The role of accommodation zones and transfer zones in the regional segmentation of extended terranes. Geol. Soc. Am. Spec. Pap. 323, 1–45. http://dx.doi.org/10.1130/0-8137-2323-X.1.
Gani, N.D., Abdelsalam, M.G., Gani, M.R., 2007. Blue Nile incision on the Ethiopian plateau: pulsed plateau growth, Pliocene uplift, and hominin evolution. GSA Today 17, 4–11.
Hayward, N.J., Ebinger, C.J., 1996. Variations in the along-axis segmentation of the Afar rift system. Tectonics 15, 244–257.
Hutchison, W., Pyle, D.M., Mather, T.A., Yirgu, G., Biggs, J., Cohen, B.E., Barfod, D.N., Lewi, E., 2016. The eruptive history and magmatic evolution of Aluto volcano: new insights into silicic peralkaline volcanism in the Ethiopian rift. J. Volcanol. Geotherm. Res. 328, 9–33.
Irvine, T.N., Baragar, W.R.A., 1971. A guide to the chemical classification of the common volcanic rocks. Can. J. Earth Sci. 8, 523–548.
Isacks, B.L., 1992. Long term land surface processes: erosion, tectonics and climate history in mountain belts. In: Mather, P. (Ed.), TERRA-1, Understanding the Terrestrial Environment. Taylor and Francis, London, UK, pp. 21–36.
Keir, D., Bastow, I.D., Pagli, C., Chambers, E., 2013. The development of extension and magmatism in the red sea rift of Afar. Tectonophysics 607, 98–114.
Keranen, K., Klemperer, S.L., 2008. Discontinuous and diachronous evolution of the main Ethiopian rift: implications for the development of continental rifts. Earth Planet. Sci. Lett. 265, 96–111. http://dx.doi.org/10.1016/j.epsl.2007.09.038.
Keranen, K., Klemperer, S.L., Julia, J., Lawrence, J.L., Nyblade, A., 2009. Low lower-crustal velocity across Ethiopia: is the Main Ethiopian Rift a narrow rift in a hot craton? Geochem. Geophys. Geosyst. 10, Q0AB01. http://dx.doi.org/10.1029/2008GC002293.
Korme, T., Acocella, V., Abebe, B., 2004. The role of pre-existing structures in the origin, propagation and architecture of faults in the main Ethiopian rift. Gondwana Res. 7, 467–479.
Laó-Dávila, D.A., Al-Salmi, H.S., Abdelsalam, M.G., Atekwana, E.A., 2015. Hierarchical segmentation of the Malawi rift: the influence of inherited lithospheric heterogeneity and kinematics in the evolution of continental rifts. Tectonics 34, 2399–2417. http://dx.doi.org/10.1002/2015TC003953.
Le Bas, M.J., le Maitre, R.W., Streckeisen, A., Zanettin, B., 1986. A chemical classification of volcanic rocks based on the total alkali-silica diagram. J. Petrol. 27, 745–750.
Le Turdu, C., Tiercelin, J.J., Gibert, E., Travi, Y., Lezzar, K.E., Richert, J.P., Massault, M., Gasse, F., Bonnefille, R., Decobert, M., Gensous, B., Jeudy, V., Tamrat, E., Mohammed, M.U., Martens, K., Atnafu, B., Cherent, T., Williamson, D., Taieb, M., 1999. The Ziway-Shala lake basin system, main Ethiopian rift: influence of volcanism, tectonics and climatic forcing on basin formation and sedimentation. Palaeogeogr. Palaeoclimatol. Palaeoecol. 150, 135–177.
Lezzar, K.E., Tiercelin, J.-J., Le Turdu, C., Cohen, A.S., Reynolds, D.J., Le Gall, B., Scholz, C.A., 2002. Control of normal fault interaction on the distribution of major Neogene sedimentary depocenters, Lake Tanganyika, east African rift. AAPG Bull. 86, 1027–1059.
McDonough, W.F., Sun, S., 1995. The composition of the earth. Chem. Geol. 120, 223–253.
Merla, G., Abbate, E., Canuti, P., Sagri, M., Tacconi, P., 1979. Geological Map of Ethiopia and Somalia and Comment with a Map of Major Landforms (Scale 1:2,000,000). Consiglio Nazionale delle Ricerche, Rome, pp. 95.
Michon, L., Merle, O., 2001. The evolution of the Massif Central rift: spatio-temporal distribution of the volcanism. Bull. Soc. Geol. Fr. 172, 201–211.
Michon, L., Sokoutis, D., 2005. Interaction between structural inheritance and extension direction during graben and depocentre formation: an experimental approach. Tectonophysics 409, 125–146.
Mohr, P.A., Potter, E.C., 1976. The Sagatu ridge dike swarms, Ethiopian rift margin. J. Volcanol. Geotherm. Res. 1, 55–71.
Moore, J.M., Davidson, A., 1978. Rift structure in southern Ethiopia. Tectonophysics 46, 159–173. http://dx.doi.org/10.1016/0040-1951(78)90111-7.
Morley, C.K., 2010. Stress re-orientation along zones of weak fabrics in rifts: an explanation for pure extension in 'oblique' rift segments? Earth Planet. Sci. Lett. 297, 667–673.
Morley, C.K., Nelson, R.A., Patton, T.L., Munn, S.G., 1990. Transfer zones in the east African rift system and their relevance to hydrocarbon exploration in rifts (1). AAPG

Bull. 74 (8), 1234–1253.
Nelson, W.R., 2009. Two-plume Dynamics Beneath the East African Rift System: A Geochemical Perspective. The Pennsylvania State University (231 pp.).
Paulsen, T.S., Wilson, T.J., 2010. New criteria for systematic mapping and reliability assessment of monogenetic volcanic vent alignments and elongate volcanic vents for crustal stress analyses. Tectonophysics 482, 16–28.
Pearce, J.A., 1982. Trace element characteristics of lavas from destructive plate boundaries. In: Thorpe, R.S. (Ed.), Andesites. John Wiley & Sons, New York, pp. 525–548.
Pérez-Gussinyé, M., Metois, M., Fernández, M., Vergés, J., Fullea, J., Lowry, A.R., 2009. Effective elastic thickness of Africa and its relationship to other proxies for lithospheric structure and surface tectonics. Earth Planet. Sci. Lett. 287, 152–167.
Philippon, M., Corti, G., Sani, F., Bonini, M., Balestrieri, M.L., Molin, P., Willingshofer, E., Sokoutis, D., Cloetingh, S., 2014. Evolution, distribution and characteristics of rifting in southern Ethiopia. Tectonics 33, 485–508. http://dx.doi.org/10.1002/2013TC003430.
Philippon, M., Willingshofer, E., Sokoutis, D., Corti, G., Sani, F., Bonini, M., Cloetingh, S., 2015. Slip re-orientation in oblique rifts. Geology 43, 147–150.
Rapprich, V., Žáčeka, V., Verner, K., Erban, V., Goslar, T., Bekele, Y., Legesa, F., Hroch, T., Hejtmánková, P., 2016. Wendo Koshe pumice: the latest Holocene silicic explosive eruption product of the Corbetti volcanic system (southern Ethiopia). J. Volcanol. Geotherm. Res. 310, 159–171.
Rosendahl, B.R., 1987. Architecture of continental rifts with special reference to East Africa. Annu. Rev. Earth Planet. Sci. 15 (1), 445–503. http://dx.doi.org/10.1146/annurev.ea.15.050187.002305.
Saria, E., Calais, E., Stamps, D.S., Delvaux, D., Hartnady, C.J.H., 2014. Present-day kinematics of the east African rift. J. Geophys. Res. Solid Earth 119, 3584–3600. http://dx.doi.org/10.1002/2013JB010901.
Sokoutis, D., Corti, G., Bonini, M., Brun, J.-P., Cloetingh, S., Mauduit, T., Manetti, P., 2007. Modelling the extension of heterogeneous hot lithosphere. Tectonophysics 444, 63–79.
Tefera, M., Chernet, T., Haro, W., Teshome, N., Woldie, K., 1996. Geological Map of Ethiopia. Geological Survey of Ethiopia, Addis Ababa.
Tommasini, S., Manetti, P., Innocenti, F., Abebe, T., Sintoni, M.F., Conticelli, S., 2005. The Ethiopian subcontinental mantle domains: geochemical evidence from Cenozoic mafic lavas. Mineral. Petrol. 84, 259–281.
Trua, T., Deniel, C., Mazzuoli, R., 1999. Crustal control in the genesis of Plio-quaternary bimodal magmatism of the main Ethiopian rift (MER): geochemical and isotopic (Sr, Nd and Pb) evidence. Chem. Geol. 155, 201–231.
Wadge, G., Biggs, J., Lloyd, R., Kendall, J.-M., 2016. Historical volcanism and the state of stress in the east African rift system. Front. Earth Sci. 4, 86. http://dx.doi.org/10.3389/feart.2016.00086.
Wolde, B., 1989. Cenozoic volcanism and rift development in Ethiopia. J. Afr. Earth Sci. 8, 99–105.
WoldeGabriel, G., Aronson, J.L., Walter, R.C., 1990. Geology, geochronology, and rift basin development in the central sector of the main Ethiopia rift. Geol. Soc. Am. Bull. 102, 439–458.
Woldetinsae, G., Götze, H.-J., 2005. Gravity field and isostatic state of Ethiopia and adjacent areas. J. Afr. Earth Sci. 41 (1–2), 103–117. http://dx.doi.org/10.1016/j.jafrearsci.2005.02.004.
Ziegler, P.A., Cloetingh, S., 2004. Dynamic processes controlling evolution of rifted basins. Earth-Sci. Rev. 64 (1–5), 1–50. http://dx.doi.org/10.1016/S0012-8252(03)00041-2.